Sixth International Symposium on Turbulence and Shear Flow Phenomena
Seoul, Korea, 22-24 June 2009

DRAG ACTING ON AN ANGLED-WAVY PLATE BY TURBULENT WATER FLOW AT A HIGH REYNOLDS NUMBER

Yoshihiko Ozaki
Dept of Mechanical and System Engineering,
Kyoto Institute of Technology
Matsugasaki, Sakyo-ku, Kyoto, 606-8585, Japan
m8623015@edu.kit.ac.jp

Naoki Yoshitake
Dept of Mechanical and System Engineering,
Kyoto Institute of Technology
Matsugasaki, Sakyo-ku, Kyoto, 606-8585, Japan
m7623062@edu.kit.ac.jp

Yoshimichi Hagiwara
Department of Mechanical and System Engineering,
Kyoto Institute of Technology
Matsugasaki, Sakyo-ku, Kyoto, 606-8585, Japan
yoshi@kit.ac.jp

ABSTRACT

Velocities have been measured in turbulent boundary-layer flow along wavy plates located on the bottom of a shallow open channel. Total drag acting on the plates has also been measured. The friction drag and pressure drag are estimated. The results show that the friction drags of the wavy plates were slightly lower than that of the flat plate. Furthermore, the increase in the pressure drag coefficient of the wavy plates was lower than that of the two-dimensional wavy wall. The pressure-drag coefficient obtained is lower than that in the case of flow at the low Reynolds number. This is different from the result obtained by Kuzan et al. These facts are due to the small-scale recirculation flow appearing intermittently.

INTRODUCTION

The reduction of drag acting on a moving body in fluid has been focused on for many years. The reduction of drag acting on a dolphin is not an exception. The streamlined body shape is naturally effective for the reduction of pressure drag; soft skin and skin folds are thought to be effective for the reduction of friction drag (Fish, 2006). Since it is difficult to measure the drag acting on swimming dolphins, experiments with models or numerical simulations should be carried out for estimating the drag.

Choi et al. (1997) and Fujimatsu et al. (2007) obtained the reduction of friction drag in silicone-rubber coatings. The pressure drag might be sufficiently low, though they did not discuss the drag in detail. Gad-el-Hak et al. (1984) measured the friction drag for the plastisol gel surfaces whose elasticity was lower than that of the silicone rubber. They also measured the deformation of the surfaces. The values of the ratio a/λ of amplitude to wavelength for the deformed surfaces were in the range of $0.026 < a/\lambda < 0.058$. The amplitude and wavelength vary with time and location; the deformation may propagate downstream, the length of deformation is limited in the transverse direction, and some ridgelines of the deformation are at angles to the main flow. These features appear occasionally and are not always reproducible. Thus it is not easy to determine the key factors of drag reduction due to compliant coatings.

A similar problem arises in the case of the skin folds. The present authors observed such folds whose ridgelines are at an angle to the body axis in a wide region of chest and abdominal skin when a bottlenose dolphin swims fast (Zhang et al., 2007). Thus we thought that the skin folds affect the drag. The noticeable skin folds may cause an increase in the pressure drag. However, the effects of the skin folds on the pressure drag and friction drag have not yet been studied in detail.

We started the measurements of total drag and friction drag for angled-wavy plates, which were the models for the folds of swimming dolphins' abdominal skins. We assumed that the skin folds do not propagate noticeably downstream because their skins and muscles are not compliant compared with the plastisol gel. Thus the surfaces of the plates take on rigid wavy surfaces.

Turbulent flows over two-dimensional sinusoidal wavy surfaces have already been discussed in some studies e.g. Kuzan et al., 1989, Hudson and Hanratty 1996, Cherukat et al., 1998, Henn and Sykes 1999, Nakagawa and Hanratty 2003, Tuan et al., 2006. The following results have been obtained from these studies: (1) Recirculation flow appears near troughs when a/λ exceeds 0.025. (2) The friction drag is slightly higher than that of the flat plate up to $a/\lambda = 0.045$. (3) The pressure drag and total drag increase noticeably with a/λ up to $a/\lambda = 0.05$. However, few studies have been conducted to investigate the effect of a Reynolds number on turbulence statistics.

We carried out measurement of drag on an angled-wavy plate in turbulent water flow in an open channel in the previous study (Yoshitake et al., 2009). We obtained the result that the friction drag was reduced slightly, which is different from the result (2) mentioned above. In addition, the increase in the pressure drag in the case of the angled-wavy plate is much lower than that of the two-dimensional wavy surface. These results were obtained only when the Reynolds number was low.

In the present study, we revise the apparatus, and carry out measurements of flow and total drag acting on the angled-wavy plate at a high Reynolds number.

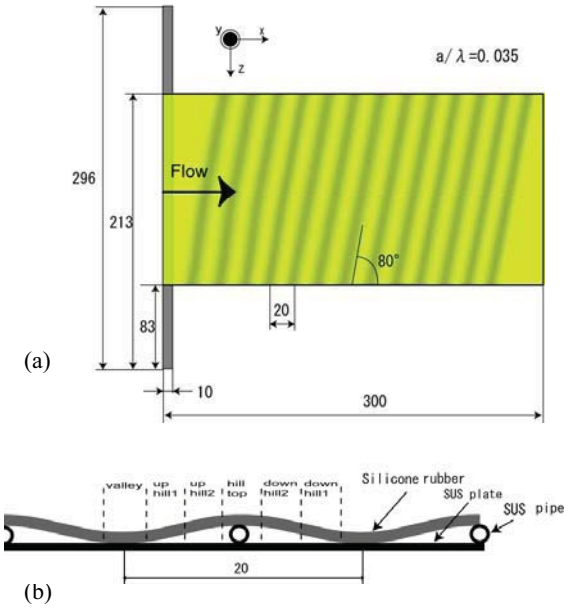

Fig. 1 Test plate: (a) configuration, (b) six sub-spaces.

EXPERIMENTAL SETUP

We built a new open channel, which is similar to that in the case of the low-Reynolds number flow (Yoshitake et al., 2009). The channel is 2000 mm in length and 270 mm in width. The bottom wall of the channel from the inlet to the downstream end of the test section was covered with a natural-rubber sheet except for the area where the test plate was positioned. A tripping wire and emery paper were placed on the rubber sheet at the channel inlet in order to promote the development of a turbulent boundary layer flow. The x and y axes were configured in the streamwise and upward directions respectively. The test section was placed at 1000 mm < x < 1300 mm.

The Reynolds number, based on the mean velocity u_e outside the turbulent boundary layer and the streamwise distance from the inlet of the channel, was 1.2×10^6. The Reynolds number based on u_e and the boundary layer thickness $\delta_{.995}$ was 1.5×10^4.

The Kolmogorov length scale l_K and Kolmogorov time scale t_K were estimated by using the friction velocity and the dissipation rate of turbulent kinetic energy. The dissipation rate near a flat wall was calculated from the DNS result obtained by Iwamoto et al (2002). l_K and t_K were 0.024 mm and 0.59 ms respectively.

We used two test plates. Each plate consisted of a T-shaped metal plate of 1.0 mm thickness, a silicone-rubber film of 0.5 mm thickness and pieces of double-sided adhesive tape. These pieces of tape were narrow in the streamwise direction and were positioned at regular intervals.

The wavy surface was formed by inserting metal pipes between the base plate and the rubber film where the latter was not fixed by the tapes. The transverse width of the plate was chosen so that the pipes could be inserted into (or pulled out from) the test plate in the water channel. The total weight of the pipes was only 2 % of the total weight of the test plate. Thus the increase in weight caused by the insertion of the pipes to the plate was negligible. The angle between the streamwise direction and the ridgelines of the wavy plate was set at 80° or 90° (hereafter called “angled” or “simple” respectively). The 80° was decided on based on not only the deformation of the compliant coatings but also the skin folds of a swimming dolphin. The angled-wavy plate is shown in Fig. 1(a). We confirmed that the shape of the rubber surface is sinusoidal-wavy. The wave amplitude a, and wavelength λ, were 0.7 mm and 20 mm respectively. Thus a/λ is 0.035. The choice of λ was based not only on the deformation of compliant coatings (Gad-el-Hak et al., 1984) but also the skin folds of a fast-swimming dolphin (Zhang et al., 2007). We divided the plate surface and the space above the surface into the following six sub surfaces and sub-spaces as shown in Fig. 1(b): valley, uphill1, uphill2, hilltop, downhill2 and downhill1.

MEASUREMENT PROCEDURES

Velocity field

We utilized tracer particles whose diameters were in the range of 0.050 - 0.060 mm, which is twice as large as l_K. The specific weight of the particles is 1.1. The upper limit of the frequency f_r, beyond which these particles cannot respond to fluid sinusoidal fluctuations completely, was estimated to be 460 Hz from the equations obtained by Hjelmfelt Jr. and Mockros (1966). The frequency corresponding to the velocity fluctuation due to the smallest eddies can be expressed by the reciprocal of the Kolmogorov time scale, which is $1/t_K$ =1700 Hz. f_r is lower than $1/t_K$. This shows that the particles cannot respond to fluctuations caused by the smallest eddies. However, f_r is nearly the same as the frequency of flow fluctuation, which can be captured by the camera mentioned below. Thus the particles adopted in the present study are reasonable.

The measurement system is shown in Fig. 2. The light of an Nd: YVO_4 laser was used as the light source. The laser beam was expanded with a plano-convex cylindrical lens and a plano-concave lens. The laser light passed through a slit of 5 mm in width above the free surface. The laser light sheet thus obtained illuminated the flow. The test plate was fixed on the bottom wall of the test section.

Scattered light from the particles was captured with a CMOS camera (Photron, FASTCAM 1024-PCI). The camera was located at one side of the channel as shown in Fig. 2. The optical axis of the camera was set parallel to the ridgelines of the wavy plates so that the valleys of the plates could be completely observed. In the case of the angled-wavy plate, a water prism was attached to the outer surface of the wall in order to reduce refraction at the channel sidewall. The captured images were slightly distorted in this case because the angle between the laser light sheet and the camera axis was 80°. We captured a reference image in order to compensate for the distortion of images. A plate with grids was used for this reference image. This plate was placed parallel to the channel axis inside the area illuminated by the laser light. Compensation of the captured images was carried out before the preprocessing of the images mentioned below. The frame rate was 1000 fps and the pixel covering area was 0.0291 × 0.0291 mm^2. The captured images were directly recorded into the memory of an interface board in a PC.

We adopted the following three-step processing of images, which is the same as that adopted in our previous studies (Kitagawa et al., 2007, Yoshitake et al., 2009):

(1) The particle-mask correlation method, developed by Etoh et al., (1999), was used to remove any weak scattered light from particles in the images.

(2) The PTV (Particle Tracking Velocimetry) technique based on the velocity gradient tensor method, proposed by Ishikawa et al., (2000), was applied to the preprocessed images for obtaining velocity vectors. In this method, the matrix including the velocity gradient tensor was calculated for pairs of neighboring particles in a specific region around a single particle.

(3) Then, the sum of the square of errors in the matrix was evaluated. This procedure was repeated for all the candidate particles until the sum reached its minimum value. This method has the advantage of accurately reproducing strongly-deformed velocity fields.

The velocities of the particles were redistributed to the grid points of 14 × 50. The velocity of a particle was simply shifted to the nearest grid point in the redistribution procedure. The uncertainty of the velocity was 0.012 m/s for u_e=1.14m/s. This shows the measured velocity was accurate.

Total drag

When the total drag was measured, the test plates were not fixed to the bottom wall. Many particles of 0.3 mm in diameter were arranged between the lower surface of the test plate and the surface of the channel in order to reduce the friction force between the test plate and the bottom of the channel.

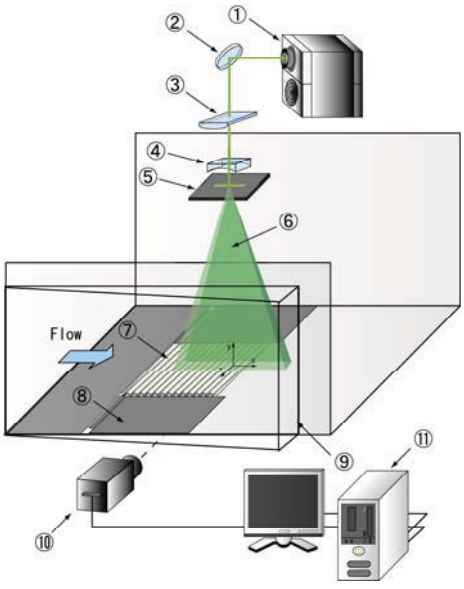

1:YVO_4 Laser, 2:Mirror, 3:Plano-convex lens. 4:Plano-concave lens, 5:Slit, 6:Laser sheet, 7:Test plate. 8:Natural rubber, 9:Prism, 10:C-MOS camera, 11:PC

Fig. 2 Velocity measurement system

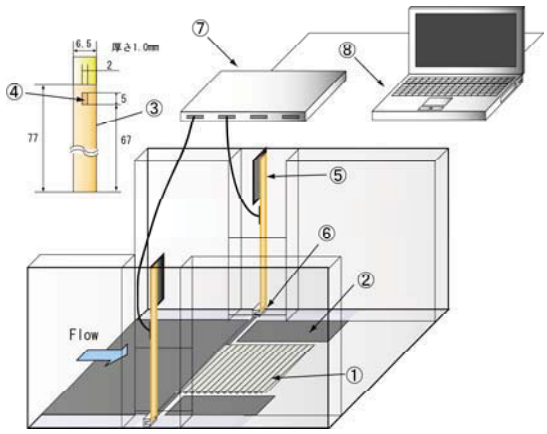

1:Test plate, 2:Natural-rubber plates, 3:Phosphor-bronze strip, 4:Strain gauge, 5:Holder, 6:U-shape mini channel, 7:Bridge circuits, 8:PC

Fig. 3 Measurement system of total drag

The measurement system for the total drag acting on the test plate is indicated in Fig. 3. The test plate was supported by two vertical cantilevers, which were made of phosphor-bronze strips. One end of each cantilever was clamped above the free surface. The other end of each cantilever made contact with an edge of a U-shaped mini channel. This mini channel was fixed to the edge of each wing of the test plate. The cantilevers were deflected slightly by the movement of the test plate due to the total drag acting on the plate. Since the measurement of the deflections in water flow is difficult, we measured the strain at the location of each cantilever by using a strain gauge. The gauges were attached to the cantilevers, and connected to bridge circuits. The outputs from the circuits were recorded on a PC. In order to reduce errors caused by the flow which collides with the cantilevers, the cantilevers were positioned inside the indented parts of the sidewall.

We carried out a calibration in order to obtain the relationship between the output from the strain gauges and the deflection of the cantilever at the loading line (i.e. the contact line of the edge of the mini channel). The cantilever was held horizontally in the air. Weights were used for changing the load at the loading line. The deflection was measured with a laser displacement sensor. The force acting on the cantilever was calculated from the deflection, the length of the cantilever and Young's modulus. The error for the total drag was approximately ±1.3%.

RESULTS AND DISCUSSION

Velocity field

Flat plate. Figure 4 shows the profile of mean streamwise velocity. The profile is found to be in agreement with that measured with a laser Doppler anemometry. The friction velocity was calculated from the gradient of mean velocity. The gradient was obtained from the fitting curve expressed with a fourth-order least square polynomial.

The profiles of turbulence intensities and Reynolds shear stress were similar to those measured by Klebanoff (in Schlichting, 1979) as shown in Fig. 5.

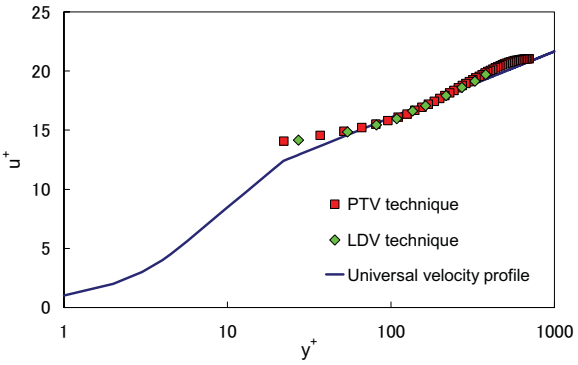

Fig. 4 Mean velocity profile for flat plate

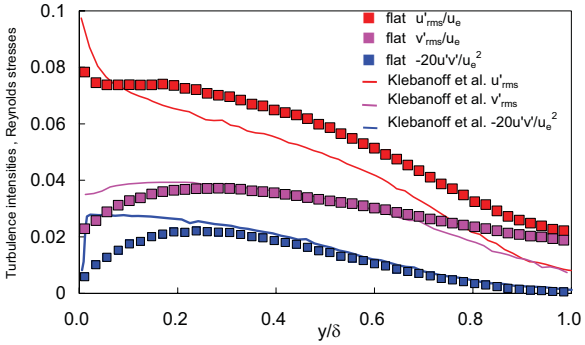

Fig. 5 Turbulence intensity and Reynolds shear stress

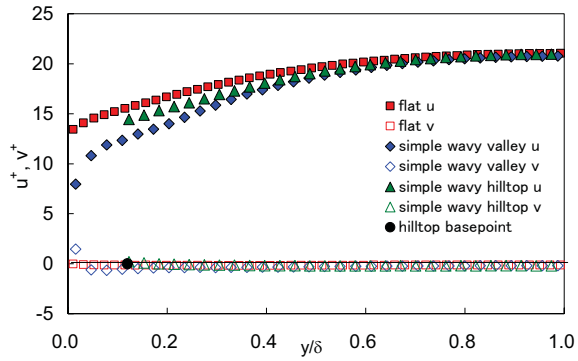

Fig. 6 Mean velocity profiles for simple wavy plate

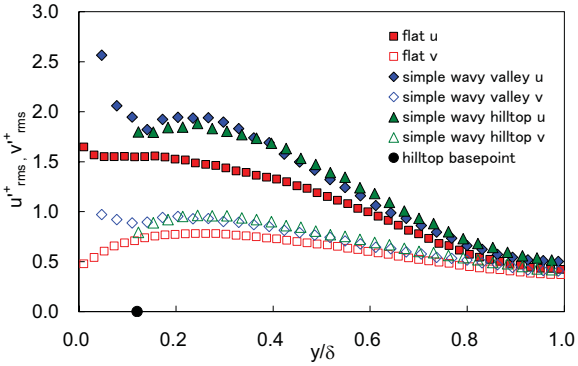

Fig. 7 Turbulence intensities for simple wavy plate

Fig.8 An image of visualized flow

Simple wavy plate. The mean velocities in the valley and hilltop regions are compared with those of the flat plate in Fig. 6 (hereafter, the friction velocity of the flat plate is used for the non-dimensional form of velocity). The former velocities are clearly lower than the latter velocity particularly near the plate surface. The boundary layer thickness was the same as that for the flat plate.

The turbulence intensities in the streamwise and vertical directions in the valley region, those in the hilltop region and those for the flat plate are compared in Fig. 7. The former two intensities are higher than the latter ones in the whole region of boundary layer. These turbulence modifications are similar to those of the turbulent open-channel flow at the low Reynolds number.

The result at the closest grid point is not shown in this figure because the uncertainty of the velocity is significant in this case. It cannot be confirmed whether or not recirculation flow occurs in the vicinity of the valley region. We visualized flow in this region by injecting dye close to the surface. Figure 8 demonstrates a typical image of the dye. A small circle of dye (indicated with an arrow) is observed in the downhill in this figure. This resulted from the recirculation flow. It should be noted that the dimension of recirculation is smaller than that observed in the case of low Reynolds number.

Effect of ridgeline angle. The effect of the ridgeline angles of the wavy plates on the flow is discussed. Figure 9 shows the profiles of streamwise mean velocity and vertical mean velocity in the valley region of the angled-wavy plate and those of the simple-wavy plate. The streamwise mean velocity in the valley region of the angled-wavy plate is equal to or slightly higher than that of the simple wavy plate.

Figure 10 exhibits the profiles of streamwise turbulence intensity and vertical turbulence intensity in the valley regions of the angled-wavy plate and simple wavy plate. The streamwise turbulence intensity of the angled-wavy plate is nearly equal to or slightly higher than that of the simple wavy plate. The vertical turbulence intensity in the case of the angled-wavy plate is slightly higher than that of the simple wavy plate. It can be concluded that the difference of 10° in the ridgeline angle slightly affects the flow above the wavy plates.

Wall shear stress

Figure 11 displays the streamwise change in the local wall-shear stress. The shear stress is divided by ρu_b^2 (ρ is the fluid density and u_b is the bulk mean velocity). x_s is the streamwise distance from the hilltop. The computational results obtained by Cherukat et al. and Henn and Sykes (a/λ = 0.025) are also shown in this figure. Cherukat et al., (1998) determined the flow separation area from the

locations of the separation and reattachment where the wall shear stress vanishes. It is found from this figure that the flow separation area is located in either $0.14 < x_s/\lambda < 0.59$ (Cherukat et al.) or $0.22 < x_s/\lambda < 0.48$ (Henn and Sykes). Thus the flow separation area expands to the downhill and valley regions.

In contrast to this, the flow separation area is not determined in the present study. This is because the recirculation flow shown in Fig. 8 appears intermittently. This intermittency results from dissipation of recirculation caused by the main flow along the edge of the wavy plates. This dissipation did not occur in the studies of other researchers (Kuzan et al., 1989, Hudson and Hanratty 1996, Cherukat et al., 1998, Nakagawa and Hanratty 2003). The wide wavy wall was in contact with sidewalls in each experiment. The periodic boundary condition gave an infinite length scale of recirculation in the transverse direction in the computations (Henn and Sykes 1999, Tuan et al., 2006).

In the computational results, the wall shear stress increases noticeably in the uphill region, while the wall shear stress increases gradually with x_s in our results as shown in Fig. 11. Cherukat et al. mentioned that a thin boundary layer originating after the reattachment point grows and accelerates under a strong pressure gradient. This acceleration by the new boundary layer causes the increase in the wall shear stress in the case of the wavy wall. Conversely, in the cases of our wavy plates, we noted that the boundary layer grows intermittently with the recirculation flow appearing intermittently. This is the reason for the low values of wall-shear stress in the uphill and hilltop regions of the wavy plates.

Total drag

The time-averaged value of the total drag D_T for the flat plate was 0.12N. The total drag should be equal to the friction drag acting on the flat plate. By assuming that the mean velocity profile is uniform over the whole surface of the flat plate, one can calculate the friction drag from the friction velocity. It was 0.12N. Thus, the measured values of total drag and friction velocity are reasonable in the case of the flat plate in the present study.

The time-averaged value of D_T for the simple wavy plate was 0.19N, while that for the angled-wavy plate was 0.18N. Thus the difference of 10° in the ridgeline angle slightly affects the total drag. The increase in D_T by forming the wavy surfaces is associated with the pressure drag due to these surfaces.

Drag coefficients

Finally, we compare the friction-drag coefficient C_F, pressure-drag coefficient C_P and total-drag coefficient C_T with those in the case of the low-Reynolds number flow. The bulk mean velocity is used to calculate these coefficients. Figures 12(a) and (b) show the values of C_F, C_P and C_T in the cases of the simple wavy plate and those of the angled-wavy plate respectively. The Reynolds numbers in the figure are based on the bulk mean velocity and water depth. The numerical result for a wavy wall at a/λ=0.035 obtained by Tuan et al. (2006) is also shown in these figures.

In Fig. 12(a), all the coefficients for the simple wavy plate in the case of the low-Reynolds number flow are found to be lower than the predicted coefficients. It is striking that the coefficients in the case of the high Reynolds number are much lower than in the other two cases. This is different from the result obtained by Kuzan et al. (1989), in which the pressure-drag coefficient increases with the Reynolds number. This difference is partly due to the inconsistency between the duct flow and the boundary-layer flow and partly due to the destabilization of the local flow structure: the approach of the shear layer to the uphill (which causes the high pressure), and the recirculation flow in the downhill and valley (which causes the low pressure), become intermittent for the present cases of wavy plates.

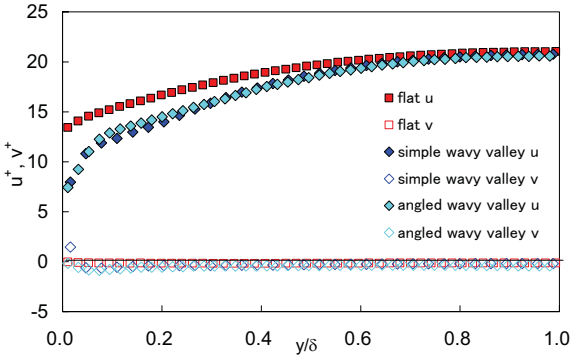

Fig. 9 Mean velocity profiles for angled-wavy plate

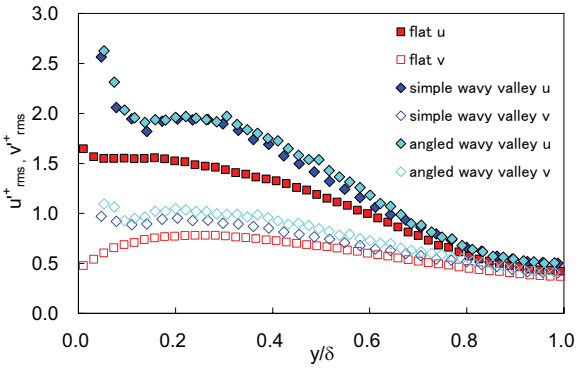

Fig. 10 Turbulence intensities for angled-wavy plate

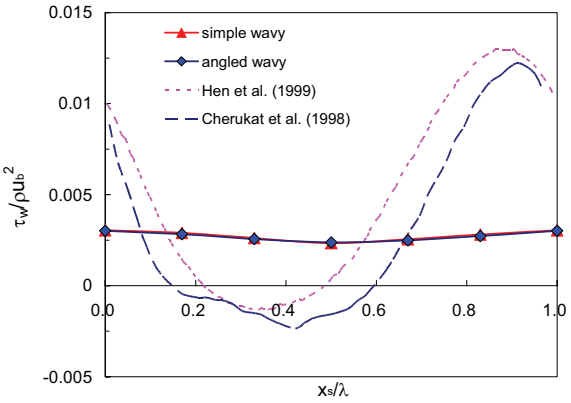

Fig. 11 Streamwise changes in wall shear stess

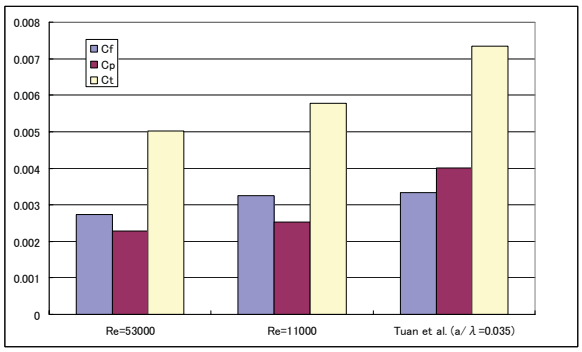

(a) simple wavy plate

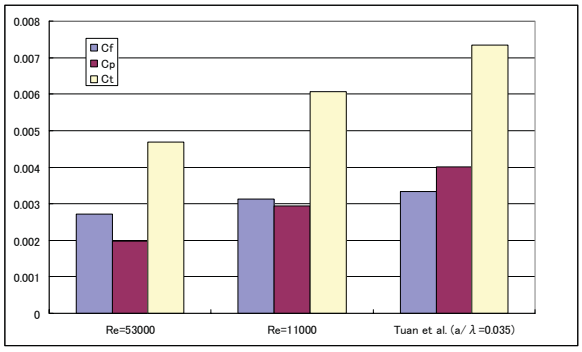

(b) angled-wavy plate

Fig. 12 Comparison of drag coefficients

All the coefficients for the angled-wavy in the case of the high Reynolds number are lower than those in the cases of the low Reynolds number and duct's wavy wall. Thus the angled-wavy surface with finite width is also effective for reducing the increase in the drags.

CONCLUSIONS

Measurements were conducted for the velocity field of turbulent boundary-layer flow along the wavy plates and total drag acting on these plates. The main conclusions obtained are as follows:

(1) The measurement methods for velocity and total drag, developed in our previous study, are effective for the turbulent boundary-layer flow at a high Reynolds number.

(2) The local values of wall shear stress show positive values even in the downhill and valley regions of the wavy plates. The coefficients of friction drag, pressure drag and total drag for the high-Reynolds number flow are lower than those for the low-Reynolds number flow and those predicted for the two-dimensional wavy wall. This is different from the result obtained from the duct flow with wavy surfaces. This is due to the fact that the small-scale recirculation flow appears intermittently. The wavy surfaces with finite width are effective for suppressing the increase in the drags.

(3) The effect of the difference of 10° in the ridgeline angle of the wavy surface is limited.

REFERENCES

Cherukat, P., Na, Y., Hanratty, T. J., and McLaughlin, J. B., 1998, "Direct numerical simulation of a fully developed turbulent flow over a wavy wall", *Theoret. Comput. Fluid Dynamics*, Vol. 11, pp. 109-134.

Choi, K. -S., et al., 1997, "Turbulent drag reduction using compliant surfaces", *Proc. Royal Soc. London* A, 453, pp. 2229-2240.

Etoh, T., Takehara, K. and Okamoto, K., 1999, "Performance evaluation of the PMC and the KC methods for particle extraction and tracking through their application to standard particle images" (in Japanese), *Trans. Japan Soc. Mech. Engrs*, Vol. 65, Ser. B, pp. 1688-1695.

Fish F. E., 2006, "The myth and reality of Gray's paradox: implication of dolphin drag reduction for technology", *J. Biomim. and Bioinsp.* Vol. 1, pp. R17-R25.

Fujimatsu, N., Misu, I., and Ishimaru, K., 2007, "Characteristics of turbulent boundary layer over silicon gel surface and behavior of surface displacement", *ASME, Proc. FEDSM2007*, Papaer No. FEDSM2007-37117, pp. 1-8.

Gad-el-Hak, M., Blackwelder, R.F. and Riley, J.J., 1984, "On the interaction of compliant coatings with boundary-layer flows", *J. Fluid Mech.*, Vol. 140, pp. 257-280.

Henn, D. S., and Sykes, R. I., 1999, "Large-eddy simulation of flow over wavy surfaces", *J. Fluid Mech.*, Vol. 383, pp. 75-112.

Hjelmfelt Jr, A. T., and Mockros, L. F., 1966, "Motion of discrete particles in a turbulent fluid", *Applied Scientific Research*, Vol. 16, pp. 149-161.

Hudson, J. D., Dykhno, L., and Hanratty, T. J., 1996, "Turbulence production in flow over a wavy wall", *Exp. in Fluids*, Vol. 20, pp. 257-265.

Ishikawa, M. et al., 2000, "A novel algorithm for particle tracking velocimetry using the velocity gradient tensor", *Exp. in Fluids*, Vol. 29, pp. 519-531.

Iwamoto, K., Suzuki, Y. and Kasagi N.,2002, "Reynolds number effect on wall turbulence: toward effective feedback control", *Int. J. Heat Fluid Flow*, Vol. 23, pp. 678-689.

Kitagawa, A., Hagiwara, Y., and Kouda, T., 2007, "PTV investigation of phase interaction in dispersed liquid-liquid two-phase turbulent swirling flow", *Exp. in Fluids*, Vol. 42, pp. 871-880.

Kuzan, J. D., Hanratty, T. J., and Adrian, R. J., 1989, "Turbulent flows with incipient separation over solid waves", *Exp. in Fluids*, Vol. 7, pp. 88-98.

Nakagawa, S., and Hanratty, T. J., 2003, "Influence of a wavy boundary on turbulence. II. Intermediate roughened and hydraulically smooth surfaces", *Exp. in Fluids*, Vol. 35, pp. 437-447.

Schlichting H., 1979, *Boundary-Layer Theory*, McGraw Hill, New York.

Tuan, H. A., El-Samni, O., Yoon, H. S., and Chun, H. H., 2006, "Immersed boundary method for simulating turbulent flow over a wavy channel", *Extended Abstracts of Whither Turbulence Prediction and Control*, pp. 116-117.

Yoshitake N., Ozaki, Y. and Hagiwara, Y., 2009a, "Drag acting on small wavy plates on the bottom of an open channel", *Int. J. Heat Fluid Flow*, submitted.

Zhang, H., Yoshitake N. and Hagiwara, Y., 2007, "Changes in drag acting on an angled wavy silicone-rubber plate as a model of the skin folds of a swimming dolphin", *Bio-mechanisms of Animals in Swimming and Flying*, N. Kato and S. Kamimura ed., Springer Verlag, Tokyo, Chapter 8, pp. 91-102.